International Journal of Geo-Information

MDPI

Article

Detecting Turning Relationships and Time Restrictions of OSM Road Intersections from Crowdsourced Trajectories

Xin Chen, Longgang Xiang *, Fengwei Jiao and Huayi Wu

State Key Laboratory of LIESMARS, Wuhan University, 129 Luoyu Road, Wuhan 430079, China
* Correspondence: geoxlg@whu.edu.cn

Abstract: OpenStreetMap (OSM) road networks provide public digital maps underlying many spatial applications such as routing engines and navigation services. However, turning relationships and time restrictions at OSM intersections are lacking in these maps, posing a threat to the accuracy and reliability of the services. In this paper, a new turn information detection method for OSM intersections using the dynamic connection information from crowdsourced trajectory data is proposed to address this problem. In this solution, the OSM intersection structure is extracted and simplified and crowdsourced trajectories are projected onto OSM road segments using an improved Hidden Markov Model (HMM) map matching method that explicitly traces the turning connections in road networks. Optimal path analysis increases the turning support related to short road segments. On this basis, this study transforms complex turning identification scenarios into the simple analyses of traffic connectivity. Furthermore, a voting strategy is used to identify and calculate turning time restrictions. The experimental results, using trajectory data from three cities in China, show that the turning relationships can be detected at a precision of 90.71% with a recall of 96.55% and an F1-value of 93.54% in Shanghai. For Wuhan, the precision is 95.33% and the recall is 95.00%, with an F1-value of 95.16%. The precision and recall when identifying turning time restrictions both reach 90% in Xiamen. These results demonstrate the effectiveness of the proposed turning detection method.

Keywords: turning relationships; map matching; turning time restrictions; OSM road networks; crowdsourced trajectories

Citation: Chen, X.; Xiang, L.; Jiao, F.; Wu, H. Detecting Turning Relationships and Time Restrictions of OSM Road Intersections from Crowdsourced Trajectories. *ISPRS Int. J. Geo-Inf.* **2023**, *12*, 372. https://doi.org/10.3390/ijgi12090372

Academic Editors: Wolfgang Kainz and Hartwig H. Hochmair

Received: 6 July 2023
Revised: 2 September 2023
Accepted: 3 September 2023
Published: 6 September 2023

1. Introduction

OpenStreetMap (OSM) is a volunteer geographic information (VGI) project founded by British engineer Steve Scott in 2004 [1]. This project has been growing rapidly, with more than 8.3 million registered users, thus realizing a global, widely, and freely used road network dataset [2]. Specifically, OSM road networks can be used in spatial analysis such as constructing building databases and the evaluation of economic development [3,4] and road obstruction [5]. In addition, these road networks support spatial applications such as identifying traffic congestion [6,7] and intelligent traffic management [8].

Among these applications, route planning and vehicle navigation services are the key areas [9], which means that the turning rule constraints must be respected in OSM road networks. Although OSM contains labels describing turning relationships at intersections [10], turn information (i.e., turning relationships and time restrictions) is significantly lacking, relative to the size of the OSM road network [11], severely threatening the accuracy and reliability of route planning and real-time traffic navigation services based on the OSM road network. More specifically, interconnected road sections found in the digital road map may actually not be connected in real traffic due to restricted turns, posing a complex and prominent problem for applications. Therefore, supplementing turn information in OSM road networks is of great practical significance.

Researchers have conducted extensive research on detecting turn information using various spatial datasets, including visual data from street scenes or mobile phone cameras [12–14], as well as crowdsourced trajectory data [13,15]. In practice, traffic signs in

images are often difficult to discern due to various factors such as inclement weather or obstructed views caused by trees or leaves. Ubiquitous crowdsourced trajectories collected by mobile devices providing location-based services, however, contain a considerable amount of dynamic traffic information. In contrast to high-quality trajectory data, crowdsourced trajectories have distinct advantages in terms of cost-effectiveness, availability, and coverage on a road network. Therefore, detecting traffic turn information from crowdsourced trajectories is a low-cost, effective, and promising approach for improved spatial applications such as routing engines and navigation services.

Detecting turn information for OSM intersections based on crowdsourced trajectories remains challenging. The number and shape of turning relationships vary at intersections due to the fact that OSM intersections consist of diverse and complex structures, making turning detection intractable. Existing studies mainly focus on clustering turning trajectories with respect to the similarity of turn-related directions or shapes [16–18]. However, the accuracy of the result depends on clustering parameters, which makes it arduous to select the appropriate parameters for the complete OSM road network. Therefore, some researchers have turned to the map matching method to assign the dynamic traffic connections of trajectories to road segments. This method uses a known road network structure to identify traffic accessibility through turning rules and therefore demonstrates greater adaptability than the clustering method [11]. However, this also raises some new issues. First, sorting out every turning connection of the target intersections from connections between any two segments still requires intensive human involvement because of the complex structures of OSM intersections, which is essential before turning rule detection; second, the anomalous semantic behaviors of trajectories caused by point drifting defies the calculation rules in map matching methods and leads to matching errors, e.g., reverse driving on a one-way segment; third, the spatial discontinuity of the matched segments corresponding to the continuous points due to low-frequency sampling interrupts turning connections, leaving certain roads, especially short segments, with insufficient turn information detection. The complicated and various structures of OSM intersections and low-quality crowdsourced trajectories increase the difficulty of turning detection, which cannot be easily resolved; furthermore, many methods concentrate on detecting the turning relationships but ignore the turning time restrictions that are also important in real-time traffic applications.

In this study, we aim to address the lack of turn information in OSM road networks. We present an intersection turning detection method that takes into account dynamic connection information of crowdsourced trajectory data based on the map matching method. Crowdsourced trajectories and OSM road networks are raw input data, and paired turning rules and turning time restrictions per hour are the output. The contributions of our research are as follows:

1. An intersection turning detection method is presented to endow road networks with turning relationships, which includes a crucial approach that simplifies OSM intersection structures. Our method transforms the complex turning identification scenarios into the uniform and simple analysis of traffic connectivity, exhibiting fine adaptability to various intersections.
2. The improved HMM map matching method is adopted to identify reverse driving sequences in terms of the valid drifting distance, which projects low-quality crowdsourced trajectories onto OSM road segments.
3. Optimum route analysis is introduced to explore the hidden turn information between the adjacent trajectory points, using travel time similarity to ensure the credibility of the found optimum route. This approach facilitates turning detection on short road segments.
4. The voting strategy is designed to extract turning time restriction information using the time series of the direct and detour turning support, which provides the quantitative detection of turning time restrictions in OSM road networks.

The rest of the study is organized as follows. Section 2 describes the previous research related to our work. Section 3 describes our method in detail. Section 4 presents the experimental results of our method. Section 5 shows the result interpretation and performance comparison of our method. Finally, Section 6 gives the conclusions and directions for future work.

2. Related Works

With the popularity of location-sensing devices, such as smart phones and vehicle-mounted GPS, crowdsourced trajectories representing the continuous spatio-temporal movements of urban residents have become a mainstay in traffic information extraction [11]. Researchers have extensively used crowdsourced trajectory-based methods to identify turn information from road intersections; these generally rely on clustering and map matching techniques.

The clustering method classifies turning trajectories according to their directional or shape similarity, and each group represents a specific turning rule at an intersection. Jing Wang et al. [19], Rong Hu et al. [16], Xiang Shuang Tan et al. [17] detected road intersections and then clustered the turning trajectories approaching the intersection coverage in terms of turning headings. Considering that turning rules with similar directions can hardly be distinguished as the result of the clustering features used, which are only related to direction, Min Deng et al. proposed a hierarchical trajectory clustering algorithm to identify turning modes [20], wherein the shape and direction features were used to measure trajectory similarity, and the Davies–Bouldin Index [21] was introduced to evaluate the selected clustering number. However, the clustering results are severely sensitive to the clustering parameters, and identifying turning relationships for specific intersections with different structures and sizes requires various clustering parameters. Therefore, it is difficult to determine and unify the common parameters to suit turning detection for all scenarios.

A handful of research projects the dynamic traffic connections of trajectories onto a road network based on the map matching method, which introduces the given intersection structures to identify the traffic accessibility of turning rules thereof. Based on the Fréchet distance curve matching method [22] and the ST matching method [23], Efentakis et al. identified the prohibited turn [11], of which the turning frequency ratio to the total number driving away the same road segment is less than the threshold. Using the map matching method considering confidence points [24], Min Huang et al. divided turning categories in advance and used the support vector machine (SVM) to perform turning classification [19]. However, these methods did not give a solution for identifying intersections and picking out the specific turning connections thereof from connections between any two segments before turning rule detection, which still requires intensive human efforts. Meanwhile, the map matching methods used pay more attention to the execution efficiency or matching accuracy facing the normal trajectories, but ignore the behavior semantic anomalies in the trajectory caused by point drifting, leading to map matching errors. Moreover, low-frequency trajectories passing through certain segments may leave no sampling points, resulting in discontinuous matched segments of continuous points, which are unavailable for turning detection. Existing methods generally filter out low-frequency subtrajectories, causing insufficient turn information detection, especially related to short segments.

In addition, the aforementioned research generally neglects turning time restrictions. The limited research with respect to time restrictions consists of one study [15], which remains a cursory analysis by displaying turning support per hour, and was inefficient when diagnosing multiple turning relationships.

3. Methodology

A workflow of the proposed method for identifying turning relationships and time restrictions of OSM intersections is shown in Figure 1, where three essential steps are illustrated. In phase 1, trajectory quality is improved by denoising and cleaning, and OSM intersection structures are simplified to facilitate turning edge detection. In phase 2,

crowdsourced trajectories are projected onto OSM road segments based on the improved HMM map matching algorithm, thereby explicitly displaying their turning processes in road networks. Considering the low-frequency sampling and uneven distribution of crowdsourced trajectories, optimum route analysis is introduced to increase support for the extraction of turning relationships on short road segments from trajectories. The turning relationships can now be identified. In phase 3, after confirming the potential time-restricted turns, the voting strategy calculates the banned traffic time of the turns. These phases will be detailed in the following subsections.

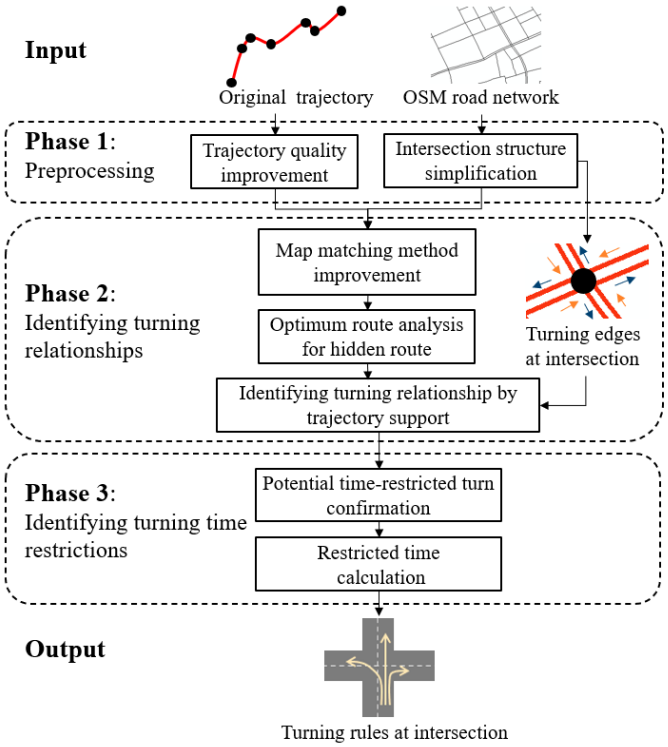

Figure 1. Workflow of the proposed method.

3.1. Preprocessing

3.1.1. Trajectory Quality Improvement

Definition 1 (trajectory). *A trajectory refers to a sequence of points recorded during a period, which is denoted as* $T = \{P_1, \ldots, P_i, \ldots, P_n\}, (0 < i < n)$*, where* $P_i = \{x_i, y_i, t_i, v_i, a_i\}$*,* x_i*,* y_i *are the longitude and latitude of* P_i *in the geographic coordinate system, respectively, and* v_i*,* a_i *are the instantaneous speed and azimuth of* P_i *sampled at timestamp* t_i*, respectively. The sampling spatial distance and time interval of two consecutive points are defined as* Δd *and* Δt*, respectively.*

Equipment failures and signal interruptions add noise and errors such as abnormal sampling and position drifting to sampling points. Meanwhile, when vehicles are stationary or moving slowly due to traffic jams, sampling points accumulate within a confined area. Trajectories collected by users in different traffic modes may also be produced when driving a nonmotor vehicle, so it is possible that trajectories could be on the reverse side of the road. These trajectory fragments are not conducive to turning relationship identification. To filter out these trajectory fragments, four preprocessing steps are introduced as follows:

1. Redundant data elimination: There are timestamp-repeated or position-repeated sampling points in the trajectory. The first points of the repeated sets are retained and the redundant data are deleted.

2. Trajectory segmentation: Due to equipment failures or signal interruptions, there is a large spatial or temporal interval between two consecutive points of trajectories. Consequently, the trajectories appear discontinuous. However, in the proposed approach, turning processes are extracted from continuous drive trajectories. Therefore, the thresholds t and d are used to cut off the trajectories ($\exists \Delta t > t$ or $\Delta d > d$).
3. Stop detection: The kernel density analysis in the literature [25] detects stop segments in a trajectory. Stop segments are simplified and represented by their geometric center point.
4. Non-motor-vehicle trajectory recognition: According to "Safety Technical Specification for Electric Bicycle (GB17761-2018)" in China [26], the maximum speed limit for driving electric bicycles is 25 km/h, which is far slower than the free-flow speed of motor vehicles. Hence, this study checks the maximum speed of trajectories throughout their lifecycle and retains the trajectory whose speed is higher than the threshold.

3.1.2. Road Intersection Simplification

The intersections in the OSM road network are extracted and turning connections are defined as the pairs of road segments connecting to the target intersection, thereby detecting the turn information from the historic paths of trajectories, using definition 2:

Definition 2 (road network). *The OSM road network is represented as a directed graph $G(E, V)$, where E is the edges of the graph and V is the vertexes of the edges, and the shared vertex of three or more edges on the ground is referred to as the cross point (CP).*

Considering that the OSM road network is drawn by different volunteers, and further, intersections have complex and diverse structures, there are various ways to express OSM intersections. Consequently, detecting OSM intersections and ascertaining the corresponding turning connections take much work. On the other hand, this study is only interested in the traffic rules between turning road segments instead of the internal structures of intersections. To this end, this study extracts and simplifies OSM intersection structures to facilitate turn information identification, as shown in Figure 2:

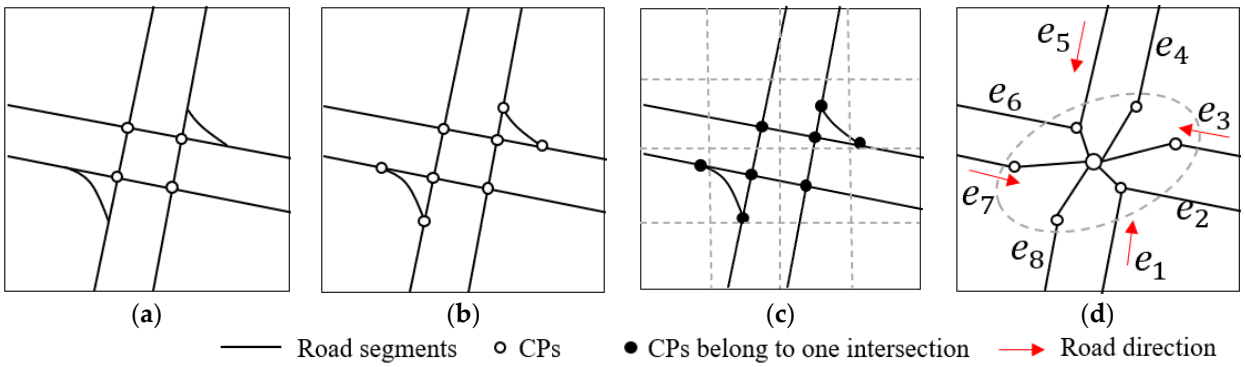

Figure 2. The process of intersection simplification: (**a**) the existing CPs; (**b**) all CPs detected after road interruption; (**c**) the CPs belong to one intersection; (**d**) the intersection is simplified as a connection point, and the road direction is derived from OSM road attributes [27].

Figure 2 illustrates the process of the method. Firstly, considering that the intersected road segments may lack the CP (see Figure 2a), the road segments on the ground are uniformly interrupted at the intersected position to detect all CPs in the road network. In OSM road networks, an intersection formed by three or more road segments either meeting or crossing could generate multiple CPs (as shown in Figure 2b, the crossroad). This study aims to discover the CPs of each intersection and integrate them into a connection point to approximately represent the intersection's position.

Subsequently, a top–down quadtree-based cell division method hierarchically splits the road network region into the smallest cells [28]. The CPs of spatial 4-neighborhood cells are grouped together (Figure 2c) and are considered to belong to one intersection. To distinguish the CPs of the adjacent intersections, referring to the minimum interval distance between intersections [29], the division is stopped when the length of the cell side is less than 50 m. Subsequently, the connection point is obtained by calculating the average coordinate of eight CPs (as shown in Figure 2d).

After simplifying the OSM intersections, the turning roads are directly connected to each other through a common connection point to intuitively show the turning connections (as listed in Table 1), facilitating turn information detection and map matching computation.

Table 1. The related turning connections of the intersection.

Intersection	Entering Roads	Leaving Roads	Examined Turning Connections
IS	$e_1, e_3,\ e_5, e_7$	$e_2, e_4,\ e_6, e_8$	$ISe_1e_2, ISe_1e_4,\ ISe_1e_6, ISe_1e_8$ etc.

3.2. Identifying Turning Relationships

3.2.1. Map Matching Method Improvement

Definition 3 (matching sequence). *$Tm = \{C_1, \ldots, C_i, \ldots, C_n\}, i \in [1, n], C_i = \{X_i, Y_i, e_i\}$, where the matched point of P_i on the road segment e_i is denoted as C_i, and X_i , Y_i are the longitude and latitude of C_i in the geographic coordinate system, respectively.*

The turn processes of the trajectories reaching intersections can be detected from their historic routes. A map matching method was introduced to combine the deviating trajectory points with the road network to recover their routes of spatial travel. The Hidden Markov Model (HMM) is a probabilistic statistical model determined by initial probability, emission probability, and transition probability distribution [30,31], and effectively integrates point positioning error, driving context distance, and driving direction in the path inference. The HMM map matching method fully considers the correlation among trajectories and road sections, thereby effectively improving the matching accuracy of low-frequency and high-noise crowdsourced trajectory data. Therefore, the HMM map matching method was adopted to restore the driving routes of trajectories.

HMM defines a system's behavior as a sequence of states $(C_1, \ldots, C_n)$, which are the hidden states of a trajectory sequence of observed states $(P_1, \ldots, P_{\mathrm{n}})$. The probability of the position C_n corresponding to a position measurement P_{n} is as follows:

$$\boldsymbol{P}(C_n) = \sum_{i=2}^{n} \boldsymbol{TP}(C_i|C_{i-1}) \cdot \boldsymbol{EP}(C_i|P_i),\ i \in [2, n] \tag{1}$$

where $\boldsymbol{P}(C_n)$ is the probability of the last position candidate C_n. The emission probability of position candidate C_i is $\boldsymbol{EP}(C_i|P_i)$ and transition probability from position C_{i-1} to position C_i is $\boldsymbol{TP}(C_i|C_{i-1})$. By employing the Viterbi algorithm, a sequence of the most likely driving positions $(C_1, \ldots, C_n)$ can be deduced when $\boldsymbol{P}(C_n)$ is the maximum value [31].

A trajectory collected by taking a car and then riding a bike may drive reversely on the road segment and can hardly be distinguished through data preprocessing. The influence of tall buildings and overpass coverings can lead to multipath interference [32], causing a point to drift to the rear of the previous point, an example of pseudo-reverse driving. This phenomenon causes matching errors; therefore, reverse driving was detected based on the constraint of the directional consistency between trajectories and roads.

To build the structure of the directed road network in map matching, two one-way roads in opposite directions were taken to signify a two-way road, considered as generally low-grade in OSM road networks. Excluding U-turns, either the driving distance of the

former of two adjacent points matched to the same one-way road is less than the latter, or the latter is driving in reverse, as shown in Figure 3.

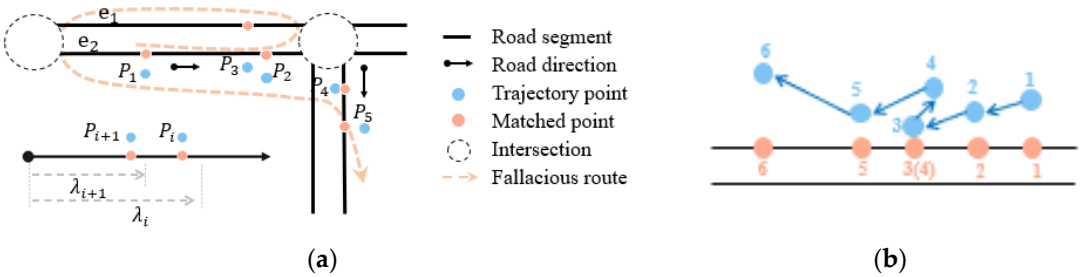

Figure 3. Identifying reverse driving with the improved map matching method: (**a**) the route from P_2 to P_3 calculated by the traditional matching algorithm concludes two U-turns (from e_2 to e_1 and then back to e_2). Conversely, the reverse-driving matched point P_3 is projected on the position of matched point of P_2 with the improved method, which makes the route more reasonable; (**b**) the matched result of a reverse driving trajectory with our method, where the number corresponds to the point index in the trajectory.

As shown in Figure 3a, P_{i+1} of T_1 is reverse driving because $\lambda_{i+1}<\lambda_i$ (that is $d_{i+1} < 0$). Moreover, this study assumes that point P_{i+1} could be deduced as pseudo-driving if the reverse drifting distance is within a threshold dv (that is $d_{i+1} < dv$); then, the transition probability of pseudo-reverse driving $\boldsymbol{TP}(C_{i+1}|C_i)_r$ of candidate C_{i+1} is added in the transition probability calculation from P_i to P_{i+1}. To ensure the reasonable matching process for normal trajectories on two-way or parallel roads, we used a penalty factor pf in $\boldsymbol{TP}(C_{i+1}\,|C_i)_r$ calculation, which is defined as follows:

$$d_{i+1} = \lambda_{i+1} - \lambda_i,\ (i \in [1, n]) \tag{2}$$

$$\boldsymbol{TP}(C_{i+1}|C_i) \sim \gamma \exp\{\ \gamma(\|P_{i+1} - P_i\| - (|\langle C_{i+1} - C_i\rangle|)\ \} \tag{3}$$

$$\boldsymbol{TP}(C_{i+1}|C_i)_r = pf * \boldsymbol{TP}(C_{i+1}|C_i)\ pf \in (0, 1) \tag{4}$$

where λ_i is the driving distance of P_i on the matched road e_1. In Equation (3), the normal transition probability of P_{i+1} from P_i is denoted as $\boldsymbol{TP}(C_{i+1}|C_i)$, and the obtained path is denoted as $\langle C_{i+1} - C_i\rangle$ and has length $|\langle C_{i+1} - C_i\rangle|$. γ is the specific parameter for the best sampling according to the literature [30]. In Equation (3), $|\langle C_{i+1} - C_i\rangle|$ is equal to d_i in reverse driving, and a small penalty factor value incurs a large penalty force.

3.2.2. Optimum Route Analysis for Hidden Routes

A course of turns in trajectories can be detected by identifying a pair of continuous turning roads in the corresponding matched sequence. However, a "leaping match" problem arises due to the low-frequency sampling of trajectories. In other words, the trajectories pass through certain road segments but leave no sampling point (as shown in Figure 4a, from C_1 to C_2), whereby the adjacent matched segments are discontinuous and the turning process is unknown. The discontinuities are invalid and excluded, leading to the insufficient detection of turn information, especially on the short segments with relatively sparse trajectory data. Therefore, optimum route analysis was adopted to complement the hidden routes for the adjacent "leaping match" points.

The shortest driving distance is the key reference factor in optimum route analysis [33], but regarding the shortest route as the optimum is still suspicious because the authenticity of the turning relationships contained remains pending, as depicted in Figure 4.

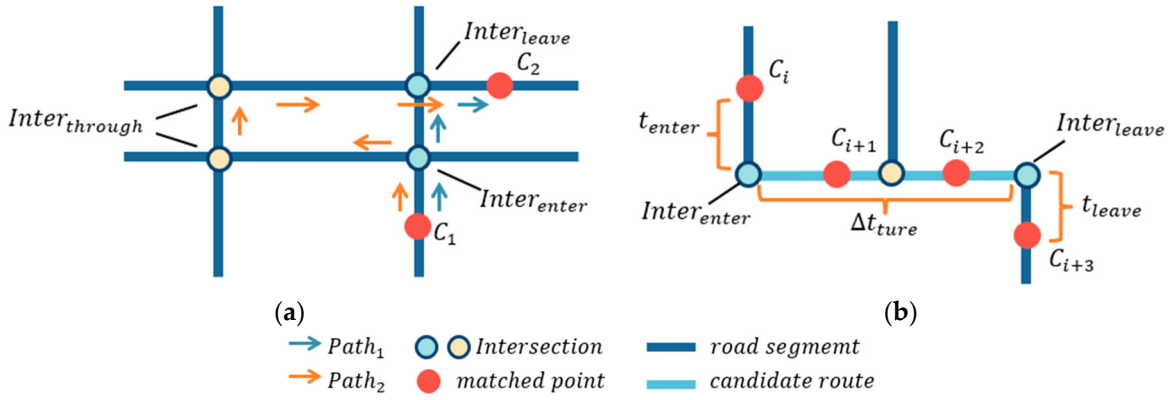

Figure 4. The driving routes and the time gaps of the adjacent matched points: (**a**) two candidate routes from C_1 to C_2, and (**b**) the real travel time of the subtrajectory on the candidate route equals $\Delta t(C_i, C_{i+3}) - t_{leave} - t_{enter}$.

where

As shown in Figure 4a, there are two available paths from C_1 to C_2, where the shortest route $path_1$ seems to be a priority; contrarily, the detour $path_2$ would be a practical selection if the right turn in $path_1$ is restriction. Therefore, referring to Bozhao Li [33], travel time is introduced to control the valid driving range of the optimum path to exclude detours. Specifically, candidate routes are calculated using the Dijkstra algorithm, part of which is discarded if the length exceeds the maximum distance allowed by travel time, assuming that the maximum limit speed in a city is 120 km/h. Nevertheless, selecting the optimum among the rest is still a difficult issue. To this end, travel time similarity is used to identify the final and reliable optimum route.

Specifically, we compared the estimated travel time (ETT) of the adjacent points with the reference travel time (RTT) of each candidate route. The route with the highest similarity degree was considered to be the reliable and optimum route. The specific travel time calculation requires further explanation. The subtrajectories that explicitly pass through a candidate path were found by observing their consecutive matched points (as shown in Figure 4b) and the real travel time thereof was obtained through the candidate route. On this basis, the RTT of the route candidate was calculated by the real travel time of subtrajectories, defined as follows:

$$RTT_k = \frac{\sum_1^n \Delta t_{ture}^q}{n} \tag{5}$$

where RTT_k denotes the RTT of the kth candidate route. Δt_{ture}^q is the real travel time of the qth subtrajectory on the candidate route, and n denotes the number of the subtrajectories obtained.

In calculating Δt_{true}, it was found that the first entering intersection and the last leaving intersection of all candidate routes of two adjacent points are fixed (as shown in Figure 4a). As a result, the candidate routes were further replaced with the paths between the two intersections. The replaced candidate routes are immune to entering intersection and leaving intersection positions of subtrajectories (as shown in Figure 4b), thereby facilitating RTT calculation using a fixed distance. In particular, this study selected the subtrajectories that were not during peak time considering that Δt_{true} would grow large because of congestion. Moreover, it was assumed that there was an even positive correlation between the driving distance and time of two adjacent points. As shown in Figure 4b, the detail Δt_{true} calculation is defined as follows:

$$\Delta t_{true} = \Delta t(C_i, C_{i+3}) - t_{leave} - t_{enter} \tag{6}$$

$$t_{leave} = \frac{Dist(C_i, Inter_{enter})}{Dist(C_i, C_{i+1})} \cdot \Delta t(C_i, C_{i+1}) \tag{7}$$

$$t_{enter} = \frac{Dist(Inter_{leave}, C_{i+3})}{Dist(C_{i+2}, C_{i+3})} \cdot \Delta t(C_{i+2}, C_{i+3}) \tag{8}$$

where $\Delta t(C_i, C_{i+3})$ denotes the sampling interval time between C_i and C_{i+3}; $Dist(C_i, C_{i+\mathrm{i}})$ is the driving distance between C_i and C_{i+1}.

Correspondingly, ETT for different candidate paths of the adjacent points (e.g., C_1 and C_2 in Figure 4a) is as follows:

$$ETT_k = \frac{Dist(Inter_{enter}, Inter_{leave})}{Dist(C_1, C_2)} \cdot \Delta t(C_1, C_2) \tag{9}$$

where ETT_k denotes the ETT of the *kth* candidate route that adjacent points (C_1, C_2) go through.

Finally, we subtracted ETT and RTT and compared their similarity for each candidate path to find the optimum route. This method introduced the real travel time for each candidate path to improve the reliability and ensures reasonable connectivity of the found optimum route.

3.2.3. Identifying Turning Relationships from Trajectory Support

After detecting turn information from the completed driving route of the matched sequence, we counted the trajectory support (TS) to identify the turn relationships of intersections. In this instance, trajectory support refers to the number of turns in trajectories crossing a target intersection. If drivers do not respect the rules of the road, then a small set of TSs are not sufficient for accurately identifying the permitted turn relationships. Therefore, referring to "consensus knowledge" and using massive crowdsourced trajectory data, an arbitrary empirical value (SUP) set at an arbitrary value to judge if a turn relationship at an intersection is permitted or forbidden. Therefore, multiple experiments were conducted to determine the optimal SUP considering the sparseness and noisiness of the trajectories. Identifying turning relationships is defined as follows:

$$(e_r, e_t) = \begin{cases} 0\mathrm{Num} < \mathrm{SUP} \\ 1\mathrm{Num} \geq \mathrm{SUP} \end{cases} r, t \in (0, \mathrm{g}) \tag{10}$$

where Num is the TS number of turning relationship (e_r, e_t). (e_r, e_t) is permitted if Num $\geq$ SUP.

Now, we can transform the complex turning identification scenarios into the uniform and simple analysis of traffic connectivity, exhibiting fine adaptability to various intersections.

3.3. Identifying Turning Time Restrictions

During peak periods, turning time restrictions are commonly implemented at intersections in urban center areas to regulate traffic order and reduce congestion. To identify these restrictions, we first analyzed the TS time series of potential time-restricted turns and then adopted a voting strategy to calculate the banned traffic time.

3.3.1. Potential Time-Restricted Turn Confirmation

Definition 4 (TS time series). *$TS_{ij}\{i \in (1, n), j \in (1, 24)\}$, where TS_{ij} is the hourly TS time series of a turning relationship, and each day is regarded as a period, so the TS at the jth time node in the ith day is denoted as TS_{ij}.*

Since most drivers are assumed to be aware of turning time restrictions but only drive illegally by accident, the TS of the banned traffic time is normally weak instead of

none. In addition, there is low throughput in the segments affected by traffic accidents or traffic jams. Therefore, it is hard to determine the threshold for time-restricted turns. However, the TS of banned traffic time is generally small and stable for certain periods. The seasonality component from time series decomposition can describe the long-term cyclical characteristics of a time series, and Dynamic Time Warping (DTW) takes the misalignment of time axis steps into account when measuring the similarity of two time series. So, DTW can efficiently measure the fluctuation of two time series of any two days. Thus, the seasonality component and DTW similarity calculations effectively reveal time-restricted turns.

Time restrictions often occur during human active times (from 6:00 a.m. to 24:00 p.m.). During this period, TS is paradoxically smaller than the rest of the times (from 0:00 a.m. to 6:00 a.m.) in the day. We identify the possible time-restricted turn if the long-term minimum of TS_{ij} is located within active times. Since the TS of the banned traffic time is periodic, small, and stable, the potential banned time is initially confirmed if the normalized seasonality component and the normalized average fluctuation thereof are both negative values.

$$j = argmin\left(\frac{\sum_{i=1}^{n} ST_{ij}}{n}\right) i \in (1,n), j \in (1,24) \tag{11}$$

where n is the number of the test periods, and the turning relationship is regarded as the possible time-restricted turn if j is located within active times.

3.3.2. Restricted Time Calculation

Considering the weak TS of the banned traffic time, there is a significant difference in the TS value between the adjacent banned traffic time node and normal time node, resulting in two distinct change points of at the boundary of each banned period. Drivers tend to take detours as the alternative during banned traffic time to complete their journeys, with the detour gaining more support as compared to the direct route. Therefore, a voting strategy was adopted to calculate the banned period exactly by considering the distinct change points and the detour TSs.

The voting flow of the banned traffic period is shown in Figure 5. We calculated the detour time series D_{ij} and the banned traffic period $block(j, j+x)_i$ of the target turning relationship.

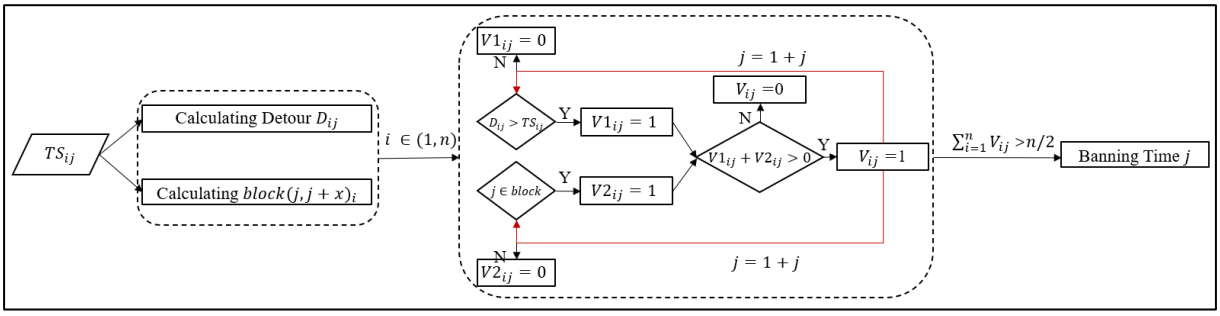

Figure 5. The voting flow of banned traffic time.

Specifically, a turning relationship could be completed by a detour consisting of multiple roads. The beginning and the ending of these roads are the real turning edges, while the remainder links to the target intersection. For example, a left turn at intersections could be completed by going straight, having a U-turn, and finally turning right (as shown in Figure 6).

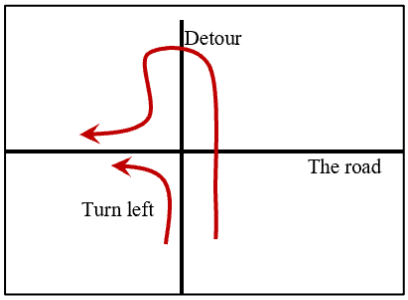

Figure 6. A detour corresponding to a direct left turn: a turning relationship could be completed by a detour consisting of multiple roads, and the red arrows are the paths of the two turns.

In addition, each banned block is determined by a pair of distinct change points, and a detailed definition is given below. Next, during the potential banned time, two voting items are further applied. The first $V1_{ij} = 1$ if the D_{ij} is greater than TS_{ij} and the second $V2_{ij} = 1$ if j in the banned block. Then, the banned traffic time of the ith day is marked as V_{ij} = 1 if at least one voting item equals 1. Finally, the banned traffic time j is confirmed if the V_{ij} of more than half of the test periods equals 1. The banned block is calculated as follows:

$$K_{ij} = \begin{cases} \begin{cases} \frac{TS_{i(j+1)} - TS_{ij}}{min\left(TS_{ij}, TS_{i(j+1)}\right)} \; min(TS_{ij}, TS_{i(j+1)}) > 0, \\ \max\left(TS_{ij}, TS_{i(j+1)}\right) min(TS_{ij}, TS_{i(j+1)}) = 0, \end{cases} & j \in [1, 23] \\ \begin{cases} \frac{TS_{(i+1)1} - TS_{ij}}{min\left(TS_{ij}, TS_{(i+1)1}\right)} \; min(TS_{ij}, TS_{(i+1)0}) > 0, \\ \max\left(TS_{ij}, TS_{(i+1)1}\right) min(TS_{ij}, TS_{(i+1)0}) = 0, \end{cases} & j = 24 \end{cases} \tag{12}$$

$$block_i = \left[index\left(min\left(K_{ij}\right)\right),\ index\left(max\left(K_{ij}\right)\right)\right] \tag{13}$$

where the TS change rate at the jth time node of the ith day is denoted as K_{ij}. K_{ij} is negative when the TS shows a downward trend, or K_{ij} is positive.

The voting strategy uses the distinct change points, and the comparison between the direct and detour turning support to extract turning time restriction information, which provides a quantitative detection for turning time restrictions in OSM road networks.

4. Experiment

In this section, the experiments used three city datasets, Shanghai, Wuhan, and Xiamen, to validate the proposed method. Specifically, we compared our proposed turn information detection method to Efentakis' method, and made a comprehensive evaluation of identifying turning relationship results for Shanghai and Wuhan. The Xiamen dataset was used to assess the turning time restriction calculations. We also explored the optimal value of SUP and evaluated the effectiveness of the improved map matching method and optimum route analysis.

4.1. Datasets and Assessment Method

Multiple experiments were conducted to excavate turn information for the OSM road network. Crowdsourced trajectories were collected from mobile phones in Shanghai and Wuhan, covering the period from 1 August 2019 to 30 August 2019, and used to detect turning relationships. After undergoing anonymization and preprocessing, the trajectories were regarded as a motor vehicle data source as shown in Figure 7; the figures on the left show the OSM road network, in which the red points are the intersections selected for evaluation, and the figures on the right show the trajectory datasets.

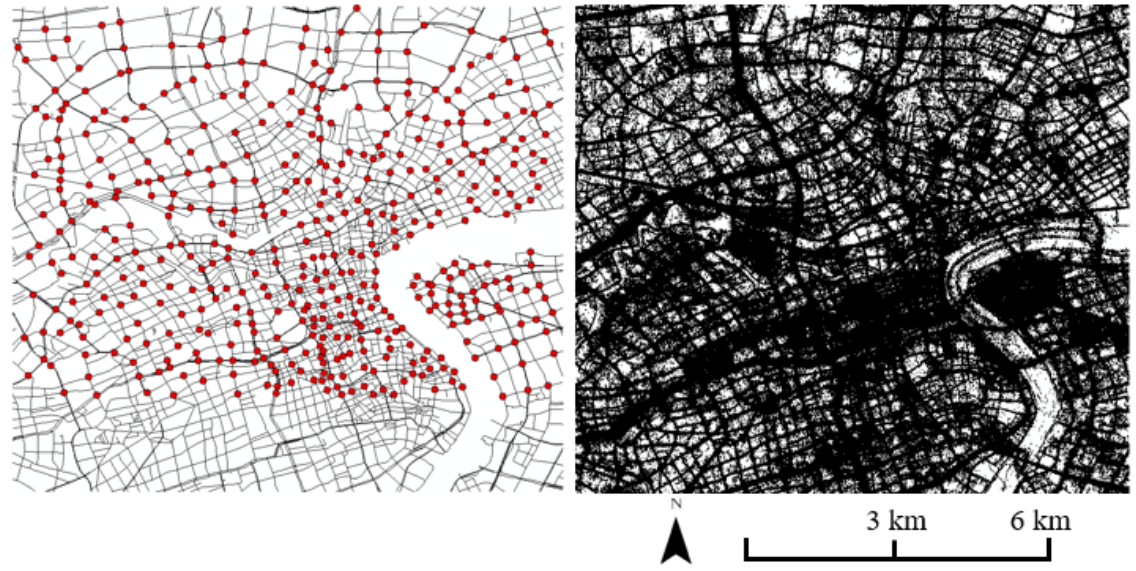

(**a**)

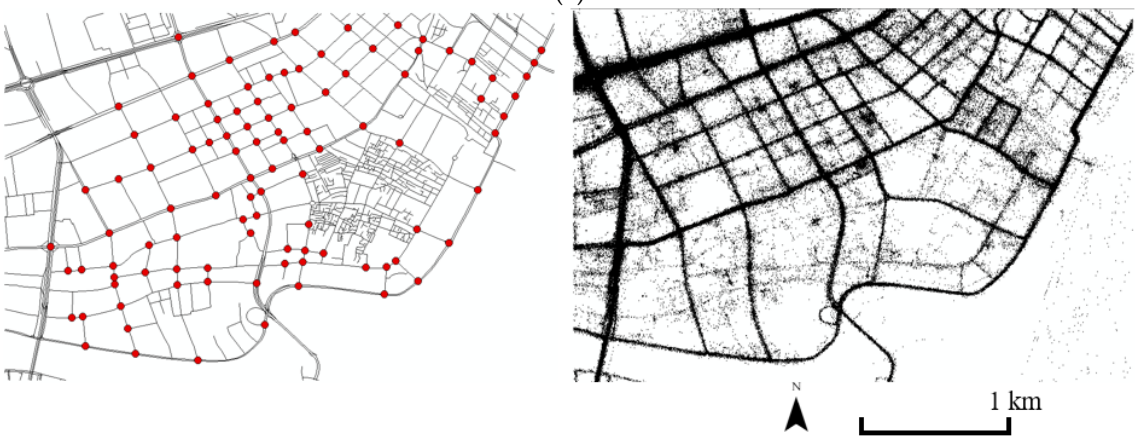

(**b**)

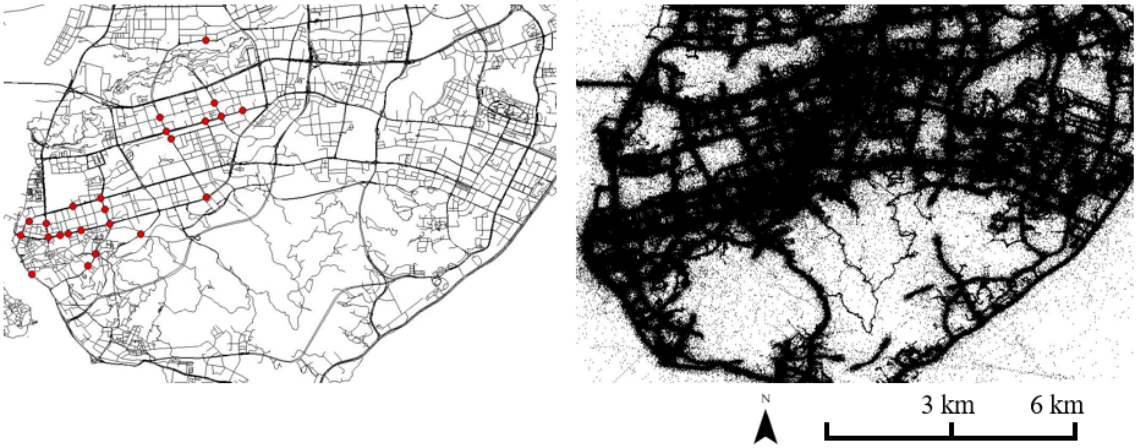

(**c**)

Figure 7. Test areas and trajectory datasets (the red points in the test area are the checked intersections): (**a**) Shanghai; (**b**) Wuhan; (**c**) Xiamen.

These three figures illustrate the test data used in our experiments. The first two, Figures a and b, show the Shanghai (Figure 7a) and Wuhan (Figure 7b) road networks. Given that the time restriction analysis based on hour granularity was sensitive to the disturbance of the few remaining non-motor-vehicle trajectories from mobile phones, we

additionally adopted crowdsourced trajectories from taxis in Xiamen (Figure 7c) to calculate turning time restriction. Each trajectory was stored in the format of record ID, timestamp, latitude, longitude, speed, and azimuth. A description of the datasets after preprocessing is shown in Table 2.

Table 2. Description of the trajectory datasets after preprocessing and the true value of turning relationships.

Cities	Test Area (km^2)	Trajectories	Trajectory Points	All Driving Lengths (km)	Time	Sampling Frequency	Tested Intersections	Positive Turns	Negative Turns	Total Turns
Shanghai	10.0 × 10.0	713,748	8,163,604	943,726	1 August 2019 to 30 August 2019	1 s to 2 min	448	4521	652	5173
Wuhan	3.5 × 2.5	17,894	215,932	23,094	1 August 2019 to 30 August 2019	1 s to 2 min	100	580	48	628
Xiamen	12.5 × 9.0	637,908	6,428,043	598,300	21 June 2020 to 25 June 2020	1 s to 2 min	24	21	410	431

The values for the tested turning relationships of the three test cities are presented in Table 2. There were 448 and 100 intersections that contained a total of 5173 pairs and 628 pairs of turning relationships in Shanghai and Wuhan, respectively. The true values of the accessible and prohibited turning relationships were confirmed based on actual traffic accessibility and labeled as positive and negative samples, respectively (as shown in Table 2). Moreover, this study examined 24 intersections in Xiamen, including 431 pairs of turning relationships. Among these, 21 pairs under time-restricted management were considered positive samples according to map street views.

Precision ($P_{positive}$), recall ($R_{positive}$), and F1-value ($F1_{positive}$) are generally used to evaluate experimental results in classification problems. Specifically, $P_{positive}$ in Formula (14) denotes the proportion of examples classified as positive that are actually positive, which measures the ability to correctly identify positive samples; $R_{positive}$ in Formula (15) is the proportion of all positive samples that are identified as positive, which measures the ability to identify positive samples; and $F1_{positive}$ is a comprehensive evaluation index that balances $P_{positive}$ and $R_{positive}$. Moreover, $F1_{weight}$ in Formula (20) weighted by the ratio of positive F1-value $F1_{positive}$ and negative F1-value $F1_{negative}$ is further introduced to evaluate turning relationship identification since the positive number is much larger than the negative. To conclude, a higher $F1_{weight}$ value indicates better experimental results. The assessment indicators are defined as follows:

$$P_{positive} = TP/(TP + FP) \tag{14}$$

$$R_{positive} = TP/(TP + FN) \tag{15}$$

$$F1_{positive} = 2 * P_{positive} * R_{positive}/\left(P_{positive} + R_{positive}\right) \tag{16}$$

$$P_{negative} = TN/(FN + TN) \tag{17}$$

$$R_{negative} = TN/(FP + TN) \tag{18}$$

$$F1_{negative} = 2 * P_{negative} * R_{negative}/\left(P_{negative} + R_{negative}\right) \tag{19}$$

$$F1_{weight} = \alpha * F1_{positive} + \beta * F1_{negative} \tag{20}$$

$$\alpha = (TP + FN)/(TP + FP + FN + TN) \tag{21}$$

$$\beta = (TN + FP)/(TP + FP + FN + TN) \tag{22}$$

where TP and FN are the number of positive samples identified as positive and negative samples, respectively, and FP and TN are the number of negative samples identified as positive and negative samples, respectively. $P_{negative}$, $R_{negative}$, and $F1_{negative}$ are the precision, recall, and F1-value of the negative samples, respectively.

4.2. Experimental Results

4.2.1. Turn information Identification

In the step of improving trajectory quality, according to the experience from previous studies [25,34], the maximum sampling frequency and sampling distance were set as 120 s and 1.5 km, respectively; the spatial radius and time duration of stop detection were set as 30 m and 60 s, respectively; and since the speed of nonmotor vehicles is usually less than 25 km/h, which is far less than the speed of the free flow of motor vehicles, the speed threshold of reserving motor vehicles was set as 25 km/h. Subsequently, to project the crowdsourced trajectories onto the road segments, we used the improved HMM map matching based on the framework provided by Yang [31] and set dv as 25 m, pf as 0.1, and γ as 0.8. To further verify the effectiveness of our method, Efentakis' method [11] was chosen as the baseline method to compare with the proposed method. The threshold in Efentakis' method was an empirical value of 5%, meaning that the TS of the permitted turn to the total number of TSs exiting from the same road segment should be higher than 5%. By contrast, the SUP in our method was initially 10. A comparison is shown in Table 3.

Table 3. Comparison of the experimental results of different methods (%).

Methods	Test Areas	$P_{positive}$	$R_{positive}$	$F1_{positive}$	$F1_{negative}$	$F1_{weight}$
Efentakis	Shanghai	89.86	74.10	81.22	26.13	74.28
	Wuhan	97.04	79.14	87.18	33.50	83.08
Our method	Shanghai	**90.71**	**96.55**	**93.54**	**40.47**	**86.85**
	Wuhan	**97.90**	**80.52**	**88.36**	**38.20**	**84.53**

Table 3 illustrates that the $P_{positive}$, $R_{positive}$, and $F1_{weight}$ of our method in Shanghai and Wuhan increased in difference degree compared with Efentakis' method. In addition, our experiment in Xiamen identified time-restricted turning relationships with both precision and recall reaching 90%. It shows that our method could comprehensively and efficiently detect turning relationships and time restrictions for OSM intersections. In the following section, we explore the best SUP for these two cities.

4.2.2. The Optimal SUP Value

To determine the best SUP value to obtain the optimal result for the turning relationship identification of OSM road networks, this study conducted a series of experiments with SUP = [2,4,6,8,10,12,14,16,18,20]. Table 4 illustrates the assessment indicators of the different experiments.

These results suggest that $F1_{weight}$ reached 86.85% when SUP = 10 in Shanghai and reached 91.16% when SUP = 4 in Wuhan, achieving the optimal result. We made two improvements in the methodology; then, we verified the effectiveness of the improved map matching method and optimum route analysis.

Table 4. Comparison of the experiments with different SUP values (%).

Test Areas	Evaluation (%)	Trajectory Support Values (SUPs)									
		2	**4**	**6**	**8**	**10**	**12**	**14**	**16**	**18**	**20**
Shanghai	$P_{positive}$	89.46	89.79	90.10	90.36	**90.71**	90.93	91.23	91.41	91.73	91.88
	$R_{positive}$	99.51	98.85	98.08	97.28	**96.55**	95.36	94.14	92.70	91.53	90.38
	$F1_{positive}$	94.22	94.1	93.92	93.69	**93.54**	93.09	92.66	92.05	91.63	91.12
	$F1_{negative}$	30.65	33.97	36.51	38.21	**40.47**	40.96	41.89	41.61	42.47	42.23
	$F1_{weight}$	86.21	86.52	86.68	86.69	**86.85**	86.52	86.26	85.69	85.43	84.96
Wuhan	$P_{positive}$	93.59	**95.33**	96.70	97.44	97.90	98.25	98.43	98.35	98.77	99.23
	$R_{positive}$	98.10	**95.00**	90.86	85.34	80.52	77.59	75.52	72.07	69.14	66.38
	$F1_{positive}$	95.79	**95.16**	93.69	90.99	88.36	86.71	85.47	83.18	81.34	79.55
	$F1_{negative}$	26.47	**42.86**	45.8	41.67	38.20	36.70	35.49	32.67	31.85	31.25
	$F1_{weight}$	90.49	**91.16**	90.03	87.22	84.53	82.89	81.65	79.32	77.56	75.86

4.2.3. Reverse Driving Identification

A sample of 2500 pseudo-reverse driving trajectories were identified to verify the effectiveness of the improved map matching method, wherein the reverse point is denoted as P_i. Compared with the previous point, the directional change in P_i and P_{i+1} is $angle_1$ and $angle_2$, respectively; the directional change in the relative displacement between P_{i-1} to P_i and P_i to P_{i+1} is $angle_3$. The directional change distribution of these points is shown in Figure 8.

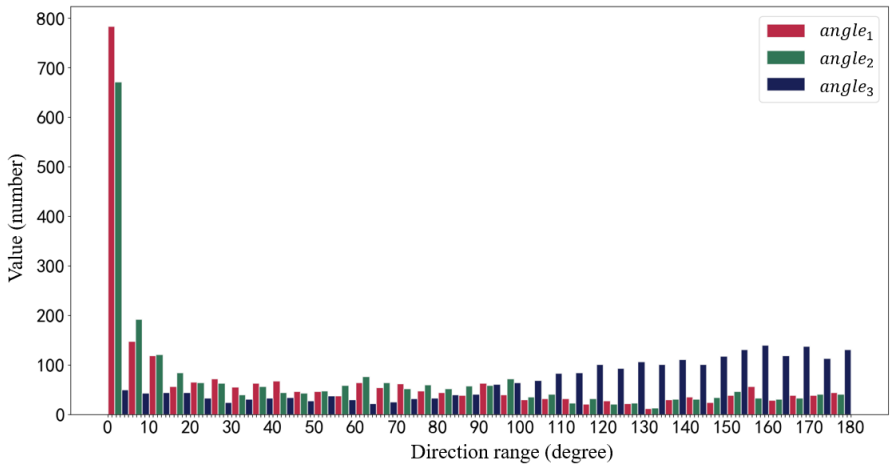

Figure 8. Distributions of $angle_1$, $angle_2$, and $angle_3$: $angle_1$ and $angle_2$ are concentrated in the area of nearly 0°, while $angle_3$ is mainly distributed in the area with large values.

As shown in Figure 8, $angle_1$ and $angle_2$ are mostly concentrated around 0°, indicating a consistency in the direction of most reverse points with their preceding and subsequent points. This alignment suggests that these three points approximately lie on a straight line. However, $angle_3$ shows a contradiction, being mainly distributed in the area with large values. This distribution suggests that most points often follow a winding path between their front and back points. The aforementioned phenomenon verified a contradiction between the original direction and the movement direction of P_i. Therefore, the improved map matching algorithm can effectively detect pseudo-reverse driving in trajectories. These three directional changes are defined as follows:

$$angle_1 = arc\ cos(a_i - a_{i-1}) * \frac{180}{\pi} i \in [0, N) \quad (23)$$

$$angle_2 = arc\ cos(a_{i+1} - a_i) * \frac{180}{\pi} i \in [0, N) \quad (24)$$

$$angle_3 = arc\ cos\left(\underset{P_{i-1}P_i}{\rightarrow}, \underset{P_iP_{i+1}}{\rightarrow}\right) * \frac{180}{\pi} i \in [0, N) \quad (25)$$

where n is the number of sampling points in the trajectory, the three points (P_{i-1}, P_i, P_{i+1}) lie on approximately one line if $angle_1$ and $angle_2$ are close to 0°, and P_i has a turnaround movement between its front and rear points if $angle_3$ approaches 180°.

4.2.4. Route Supplement Results

We compared the experimental results between using a route supplement and no route supplement in Shanghai when SUP = 10 and in Wuhan when SUP = 4. The details are as shown in Table 5.

Table 5. Comparison of the experiments of different cities with different approaches (%).

Test Areas	Approaches	$P_{positive}$	$R_{positive}$	$F1_{positive}$	$F1_{negative}$	$F1_{weight}$
Shanghai (SUP = 10)	No Route Supplement	93.76	69.74	79.99	35.91	74.43
	Route Supplement	**90.71**	**96.55**	**93.54**	**40.47**	**86.85**
Wuhan (SUP = 4)	No Route Supplement	96.56	82.24	88.83	34.06	84.64
	Route Supplement	**95.33**	**95.00**	**95.16**	**42.86**	**91.16**

After conducting optimum route analysis for the hidden turn information, a noteworthy enhancement in $\boldsymbol{R_{positive}}$ was obtained while maintaining high $\boldsymbol{P_{positive}}$ values. Specifically, $\boldsymbol{R_{positive}}$ increased by 26.81% in Shanghai and 12.76% in Wuhan, respectively. Moreover, as shown in Figure 9, $\boldsymbol{F1_{positive}}$, $\boldsymbol{F1_{negative}}$, and $\boldsymbol{F1_{weight}}$ also increased to different extents in both cities, which indicates that conducting a route supplement can identify turning relationships more completely.

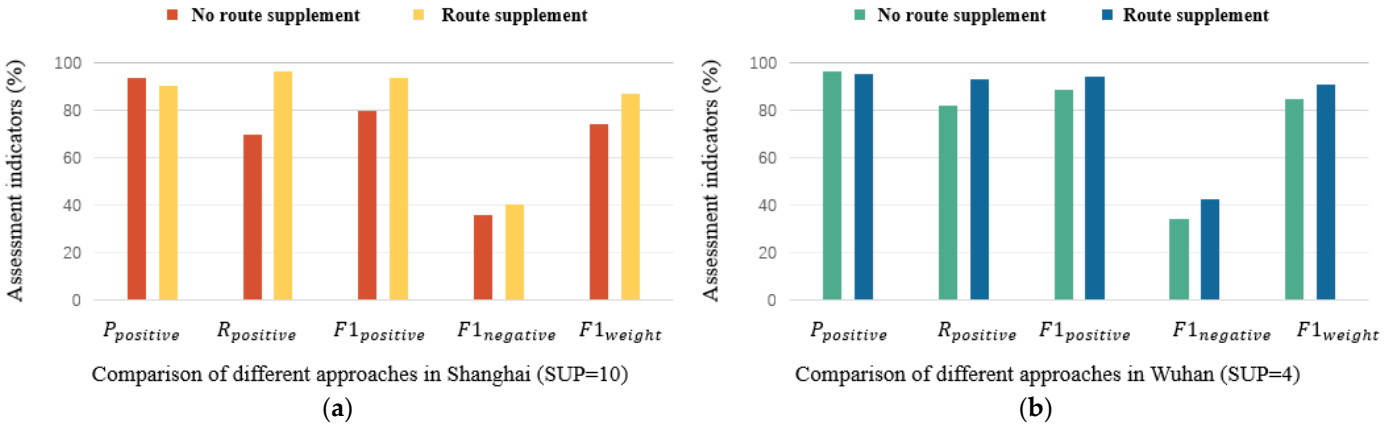

Figure 9. Comparison of the experiments with different approaches in different areas: (**a**) Shanghai and (**b**) Wuhan.

5. Discussion

Based on low cost, fast updating, and high-coverage crowdsourced trajectory data, this proposed method could comprehensively and efficiently detect the turning relationships and time restrictions of OSM road network intersections. Specifically, our method is superior to Efentakis' method (as detailed in Table 3, Section 4.2.1). Efentakis' method ignores the problem of "leap matching" and semantic anomalies of trajectories, performing poorly on short roads with relatively sparse trajectories, e.g., Figure 10c illustrates two undetected turns on short segments.

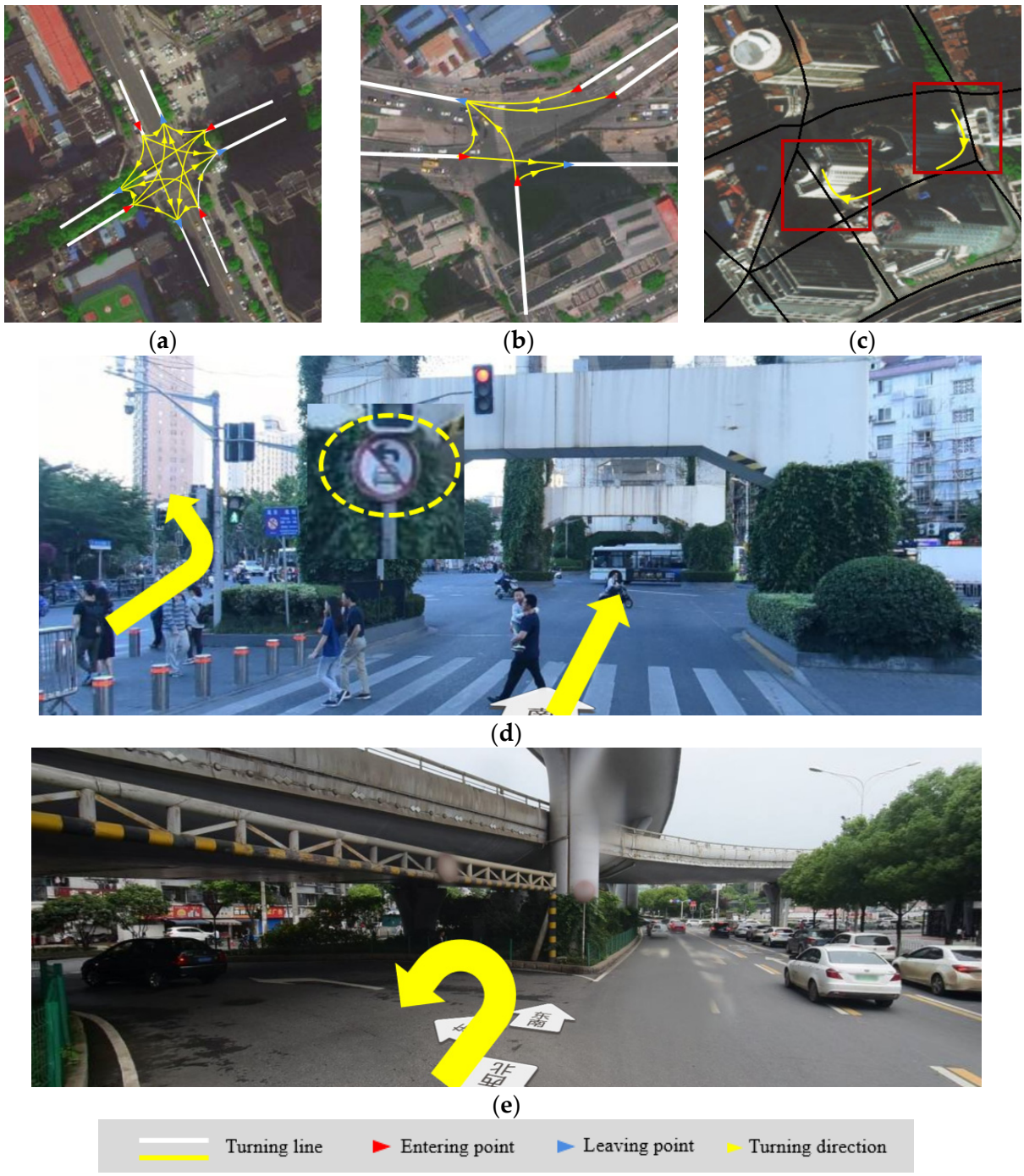

Figure 10. Examples of the identified turning relationships at intersections: (**a**) a crossroad; (**b**) a complex intersection; (**c**) the yellow turning curves related to the short road segments in the red box cannot be detected by Efentakis' method; (**d**) an intersection with parallel or same-directional road segments; (**e**) U-turns in the middle of road segment.

We achieved the best result of identifying turning relationships with SUP = 10 in Shanghai and SUP = 4 in Wuhan. It was found that the optimal SUP in Shanghai was greater than in Wuhan. We learned that the judgment condition of the permitted turns became stricter as the SUP grew, resulting in the higher precision and lower recall of positive samples. The coverage of trajectory data in Shanghai was higher than in Wuhan (see Figure 7, Section 4.1), whereby increasing the SUP had less impact on the recall rate

in Shanghai than in Wuhan. In summary, the larger the trajectory quantity, the higher the SUP can be set.

Figure 10 shows the recognized turning relationships at typical intersections. The common crossroad in Figure 10a contains 16 groups of turning relationships, and the complex and multidirectional intersection in Figure 10b involves 6 groups. The results prove that the proposed method can completely and accurately detect the turning relationships of intersections with various structures.

In addition to the error in manually marking true values, the main cause of misidentification is the incomplete filtering of non-motor-vehicle trajectories, resulting in an increase in illegal turns. As shown in Figure 10d, a vehicle from the road segment labeled with a straight arrow cannot turn left, but the other one labeled with a left arrow is permitted to do so. Therefore, the turning rules of these roads are easily confused since map matching struggles to distinguish trajectories on closely parallel or same-directional road segments, which inherently introduces errors.

There are several reasons for undetectable turning relationships. The primary one is that the turning relationships on road segments with few or no trajectory data cannot be easily identified. Moreover, there are U-turns at the middle of road segments instead of the corresponding intersection. This leads to a low U-turn frequency at intersections (as shown in Figure 10e) and the U-turns consequently remain undetected.

Figure 11 presents five intersections (a, b, c, d, and f) where time-restricted turns are thoroughly and accurately identified. This suggests that time-restricted management is generally addressed to left turns to maintain traffic flow during peak periods. However, there is an incorrect result of the calculated banned traffic time (see Figure 11e), and the specific banned traffic times are given in Table 6.

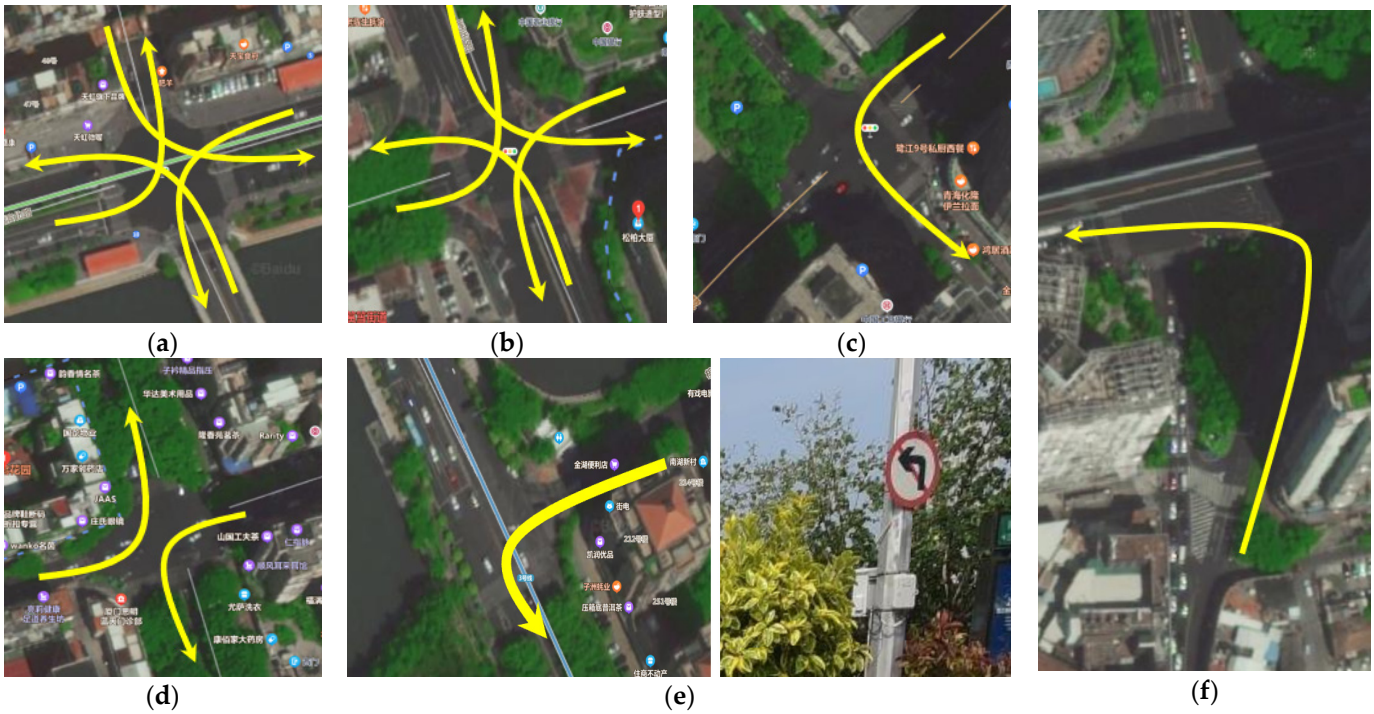

Figure 11. The identified time-restricted turning relationships at different intersections, where the yellow arrow is the time-restricted turning relationships: (**a**–**d**) crossroads; (**e**) intersection with wrong result; (**f**) a special intersection.

Table 6. Examples of the calculated banned traffic time.

Turning Relationships	Our Method	True Values
Intersection (a), (b), (c), (d), and (f)	[7:00, 22:00]	[7:00, 24:00]
Intersection (e)	[6:00, 22:00]	[0:00, 24:00]

As shown in Table 6, the obtained banned traffic time in Figure 11e does not conform to the true value. It was found that there were many trajectories passing during [0:00, 6:00], so we speculated that violating traffic rules incurs no penalties late at night, during which most vehicles select the turn directly, leading to miscalculation by our method.

In general, the error of the proposed method mainly came from three reasons: interference was caused by the remaining non-motor-vehicle trajectories; map matching errors occurred due to the large drifting distance of the sampling points; and the absence of turning trajectories led to insufficient support. Notwithstanding its limitation, the proposed method can effectively and practicably enhance turn information in the OSM road network and promote OSM applications.

6. Conclusions and Future Work

To address the lack of turning relationships and time restrictions of OSM intersections, a turn information detection method is proposed using the dynamic connection information of crowdsourced trajectory data based on the map matching method. Complex OSM intersections are identified and unified as connection points; then, low-quality and high-noise crowdsourced trajectories are projected onto OSM road segments using the improved HMM map matching method. Optimum route analysis is introduced to deal with the "leaping match" problem. On this basis, the intricate study identifying turning relationships is ultimately transformed into concise connectivity judgment. Moreover, a voting strategy utilizing the time series of the direct and detour turning support is presented to excavate turning time restrictions.

The experiments in Shanghai, Wuhan, and Xiamen show that:

1. The proposed method can effectively and completely identify turning relationships of OSM intersections with different sizes and structures. When SUP = 10, the precision, recall, and F-value reach 91%, 97%, and 94% in Shanghai; for Wuhan, the precision is 98% and the recall is 81%, with an F1-value of 88%. Our method outperforms the Efentakis method.
2. The improved HMM map matching algorithm can effectively identify reverse driving sequences, alleviating the impact caused by trajectory matching errors in turning detection.
3. Optimum route analysis for the hidden turn information promotes the integrity of turning relationship identification. The recall increases by 26.81% in Shanghai and 12.76% in Wuhan, respectively.
4. The proposed voting strategy can quantitatively reveal turning time restrictions for crucial intersections, achieving both high precision and recall.

In our future work, turning relationships at the lane level for high-definition maps will be further explored. In addition, given the interference from disorderly non-motor-vehicle trajectory driving on the road, future research will take the speed, acceleration, and stop ratio of trajectories into account to focus on traffic pattern classification for crowdsourced trajectories from multitype mobile devices.

Author Contributions: Conceptualization, Xin Chen, Longgang Xiang, Fengwei Jiao; methodology, Xin Chen; software, Xin Chen, Fengwei Jiao; validation, Xin Chen, Longgang Xiang, Fengwei Jiao; formal analysis, Xin Chen, Fengwei Jiao; investigation, Xin Chen; resources, Longgang Xiang; data curation, Xin Chen; writing—original draft preparation, Xin Chen; writing—review and editing, Xin Chen, Longgang Xiang; visualization, Xin Chen; supervision, Longgang Xiang, Huayi Wu; project administration, Longgang Xiang; funding acquisition, Longgang Xiang. All authors have read and agreed to the published version of the manuscript.

Funding: This paper was funded by the National Natural Science Foundation of China under grant No. 42071432.

Data Availability Statement: We express our thanks to the anonymous reviewer for constructive comments.

Conflicts of Interest: The authors declare no conflict of interest.

References

1. Zhang, Y.; Li, X.; Wang, A.; Bao, T.; Tian, S. Density and diversity of OpenStreetMap road networks in China. *J. Urban Manag.* **2015**, *4*, 135–146. [CrossRef]
2. OpenstreetMap. Stats. Available online: https://wiki.openstreetmap.org/wiki/Stats (accessed on 30 October 2022).
3. Liu, B.; Shi, Y.; Li, D.J.; Wang, Y.D.; Fernandez, G.; Tsou, M.H. An Economic Development Evaluation Based on the OpenStreetMap Road Network Density: The Case Study of 85 Cities in China. *ISPRS Int. J. Geo-Inf.* **2020**, *9*, 517. [CrossRef]
4. Tian, Y.J.; Zhou, Q.; Fu, X.L. An Analysis of the Evolution, Completeness and Spatial Patterns of OpenStreetMap Building Data in China. *ISPRS Int. J. Geo-Inf.* **2019**, *8*, 35. [CrossRef]
5. Wilson, B.; Allstadt, K.E.; Thompson, E.M. A near-real-time model for estimating probability of road obstruction due to earthquake-triggered landslides. *Earthq. Spectra* **2021**, *37*, 2400–2418. [CrossRef]
6. Ghosh, S.; Chowdhury, A.; Ghosh, S.K. A Machine Learning Approach to Find the Optimal Routes Through Analysis of GPS Traces of Mobile City Traffic. In Proceedings of the 5th International Conference on Advanced Computing, Networking, and Informatics (ICACNI), Goa, India, 1–3 June 2017; pp. 59–67.
7. Zhang, Z.G.; Ming, Y.; Song, G.B. A New Approach to Identifying Crash Hotspot Intersections (CHIs) Using Spatial Weights Matrices. *Appl. Sci.* **2020**, *10*, 1625. [CrossRef]
8. Khumara, M.A.D.; Fauziyyah, L.; Kristalina, P. Estimation of Urban Traffic State Using Simulation of Urban Mobility (SUMO) to Optimize Intelligent Transport System in Smart City. In Proceedings of the IEEE International Electronics Symposium on Engineering Technology and Applications (IES-ETA), Bali, Indonesia, 29–30 October 2018; pp. 163–169.
9. Tabet, F.; Pentyala, S.; Patel, B.H.; Hendawi, A.; Cao, P.W.; Song, A.; Govind, H.; Ali, M. OSMRunner: A System for Exploring and Fixing OSM Connectivity. In Proceedings of the 22nd IEEE International Conference on Mobile Data Management (IEEE MDM), Toronto, ON, Canada, 15–18 June 2021; IEEE: Piscataway, NJ, USA, 2021; pp. 193–200.
10. OpenstreetMap. Relation: Restriction. Available online: https://wiki.openstreetmap.org/wiki/Relation:restriction (accessed on 30 October 2020).
11. Efentakis, A.; Grivas, N.; Pfoser, D.; Vassiliou, Y. Crowdsourcing turning-restrictions from map-matched trajectories. *Inf. Syst.* **2016**, *64*, 221–236. [CrossRef]
12. Campbell, A.; Both, A.; Sun, Q. Detecting and mapping traffic signs from Google Street View images using deep learning and GIS. *Comput. Environ. Urban Syst.* **2019**, *77*, 101350. [CrossRef]
13. Naseer, M.; Supriadi, I.; Supangkat, S.H. Feature Detection of Curve Traffic Sign Image on The Bandung—Jakarta Highway. In Proceedings of the 2nd International Conference on Computing and Applied Informatics, Medan, Indonesia, 28–30 November 2017; IOP: Bristol, UK, 2018.
14. Bruno, D.R.; Osorio, F.S. Image classification system based on Deep Learning applied to the recognition of traffic signs for intelligent robotic vehicle navigation purposes. In Proceedings of the 14th Latin American Robotics Symposium (LARS)/5th Brazilian Robotics Symposium (SBR), Curitiba, Brazil, 8–11 November 2017.
15. Jing, W.; Chaoliang, W.; Xianfeng, S.; Venkatesh, R. Automatic intersection and traffic rule detection by mining motor-vehicle GPS trajectories. *Comput. Environ. Urban Syst.* **2017**, *64*, 19–29. [CrossRef]
16. Hu, R.; Xu, Y.; Chen, H.; Zou, F. A novel method for the detection of road intersections and traffic rules using big floating car data. *IET Intell. Transp. Syst.* **2022**, *16*, 983–997. [CrossRef]
17. Tan, X.; Wang, J.; Song, X.; Xu, C.; Wang, C. Detection of Road Intersections Using Floating Car Data. *Geogr. Geo-Inf. Sci.* **2015**, *31*, 34–38.
18. Yu, Q.Y.; Hu, F.; Chen, C.M.; Sun, L.P.; Zheng, X.Y. Low-Frequency Trajectory Map Matching Method Based on Vehicle Heading Segmentation. *ISPRS Int. J. Geo-Inf.* **2022**, *11*, 355. [CrossRef]
19. Huang, M.; Pan, J.; Liu, F. Modeling for logical connectivity of intersection based on SVM. *Comput. Eng. Des.* **2017**, *38*, 1319–1323. [CrossRef]

20. Deng, M.; Huang, J.; Zhang, Y.; Liu, H.; Tang, L.; Tang, J.; Xuexi, Y. Generating urban road intersection models from low-frequency GPS trajectory data. *Int. J. Geogr. Inf. Sci.* **2018**, *32*, 2337–2361. [CrossRef]
21. Davies, D.L.; Bouldin, D.W. A Cluster Separation Measure. *IEEE Trans. Pattern Anal. Mach. Intell.* **1979**, *PAMI-1*, 224–227. [CrossRef]
22. Brakatsoulas, S.; Pfoser, D.; Tryfona, N. On map-maching vehicle tracking data. In Proceedings of the 31st International Conference on Very Large Data Bases, Trondheim, Norway, 30 August–2 September 2005; pp. 324–325.
23. Lou, Y.; Zhang, C.; Zheng, Y.; Xie, X.; Wang, W.; Huang, Y. Map-Matching for Low-Sampling-Rate GPS Trajectories. In Proceedings of the GIS' 09: 17th ACM SIGSPATIAL International Conference on Advances in Geographic Information Systems, Seattle Washington, DC, USA, 4–6 November 2009; pp. 352–361. [CrossRef]
24. He, Z.-c.; She, X.-w.; Zhuang, L.-j.; Nie, P.-l. Online Map-Matching Framework for Floating-Car Data with Low Sampling Rate in Urban Road Networks. *IET Intell. Transp. Syst.* **2012**, *7*, 404–414. [CrossRef]
25. Xiang, L.G.; Gao, M.; Wu, T. Extracting Stops from Noisy Trajectories: A Sequence Oriented Clustering Approach. *ISPRS Int. J. Geo-Inf.* **2016**, *5*, 29. [CrossRef]
26. Safety Technical Specification for Electric Bicycle (GB17761-2018). Available online: https://www.yunfu.gov.cn/yfgxj/gkmlpt/content/1/1592/post_1592759.html#4531 (accessed on 30 October 2022).
27. OpenstreetMap. Zh-hans: Map_Features. Available online: https://wiki.openstreetmap.org/wiki/Zh-hans:Map_Features#%E5%B1%9E%E6%80%A7 (accessed on 10 August 2023).
28. Zhao, L.; Mao, J.; Pu, M.; Liu, G.; Chai, H. Automatic Calibration of Road Intersection Topology using Trajectories. In Proceedings of the 2020 IEEE 36th International Conference on Data Engineering (ICDE), Dallas, TX, USA, 20–24 April 2020; pp. 1633–1644.
29. Zhang, C.L.; Xiang, L.G.; Li, S.Y.; Wang, D.H. An Intersection-First Approach for Road Network Generation from Crowd-Sourced Vehicle Trajectories. *ISPRS Int. J. Geo-Inf.* **2019**, *8*, 473. [CrossRef]
30. Mattheis, S.; Al-Zahid, K.K.; Engelmann, B.; Hildisch, A.; Zinck, R.D. *Putting the Car on the Map: A Scalable Map Matching System for the Open Source Community*; Informatik: Stuttgart, Germany, 2014.
31. Yang, C.; Gidofalvi, G. Fast map matching, an algorithm integrating hidden Markov model with precomputation. *Int. J. Geogr. Inf. Sci.* **2018**, *32*, 547–570. [CrossRef]
32. Zhai, Y.; Weng, J.; Rong, J.; Liu, X. Experimental based traffic flow detectors data accuracy evaluation. *J. Beijing Univ. Aeronaut. Astronaut.* **2011**, *37*, 733.
33. Li, B.; Cai, Z.; Kang, M.; Su, S.; Jiang, L.; Ge, Y.; Niu, Y. An improved hidden Markov model-based map matching algorithm considering candidate point grouping and trajectory connectivity. *Cartogr. Geogr. Inf. Sci.* **2023**, *50*, 351–370. [CrossRef]
34. Zhang, C.; Li, Y.; Xiang, L.; Jiao, F.; Wu, C.; Siyu, L. Generating Road Networks for Old Downtown Areas Based on Crowd-Sourced Vehicle Trajectories. *Sensors* **2021**, *21*, 235. [CrossRef] [PubMed]